MICROBOONE-NOTE-1115-PUB

Demonstration of <2 ns timing resolution for neutrino interaction in the MicroBooNE detector

The MicroBooNE Collaboration

MICROBOONE_INFO@fnal.gov

May 27, 2022

Abstract

The MicroBooNE detector, located in the Booster Neutrino Beamline (BNB) at Fermilab, collected data from 2015 to 2021. MicroBooNE's Liquid Argon Time Projection Chamber is accompanied by a Photon Detection System consisting of 32 PMTs used to measure the argon scintillation light and determine the timing of the neutrino interactions. This work employs improved analysis techniques combining light signals and reconstructed tracks achieving neutrino interaction timing resolution <2 ns. The result obtained allows MicroBooNE to access the 2 ns neutrino pulse structure of the BNB for the first time. The timing resolution achieved enables significant enhancement of cosmic background rejection for all neutrino analyses. Furthermore, the ns timing resolution opens the door for searching new long-lived-particles (e.g. Heavy Neutral Leptons, Higgs Portal Scalars) in MicroBooNE, as well in future large LArTPC experiments, namely SBN and DUNE.

Contents

1 Introduction

This note reports the analysis techniques developed to improve the neutrino interaction timing resolution of the MicroBooNE detector [1]. Combining light signals and reconstructed tracks, a <2 ns timing resolution is achieved and the neutrino pulse ns substructure of the Booster Neutrino Beamline (BNB) has been resolved for the first time in MicroBooNE. The scintillation light prompt signal provided by the Photon Detection System (PDS) [2] is used to observe the BNB pulse substructure after several calibration and reconstruction steps are applied. A jitter in the BNB main trigger is removed using the signal provided by the resistive wall current monitor (RWM) located immediately before protons hit the target. The time of flight (ToF) of neutrinos inside the detector, as well as daughter particles and scintillation light photons are reconstructed leveraging the ν interaction vertex and particle tracks geometry provided by the Time Projection Chamber (TPC). Finally an empirical calibration is used to apply corrections on the combined daughter particles plus scintillation light propagation time. The neutrino sample used is an inclusive selection of ν_μCC interactions candidates [3] from the BNB events from MicroBooNE's Run 3, which contains a $\mathcal{O}(80\%)$ pure sample of neutrino interactions.

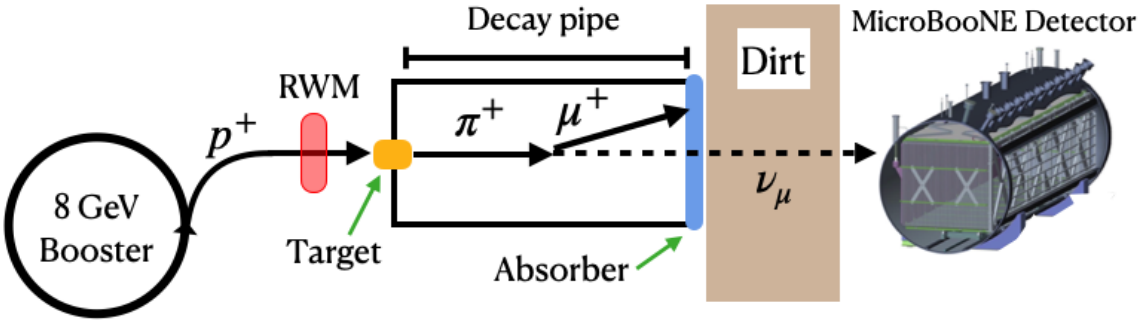

Figure 1: MicroBooNE's detector is in the path of the BNB, on axis with the beam direction, ~470 m downstream from the neutrino production target.

2 Booster Neutrino Beamline

The main source of neutrinos in the MicroBooNE experiment is the BNB [4]. The beam delivers 8 GeV (kinetic energy) proton pulses to the target. Each ~1.6 μs pulse has a 52.81 MHz microstructure that is composed of 81 bunches, and each bunch has a full width half maximum of ~2 ns [5] ($\langle\sigma_B\rangle$ =1.308 ns, STD$_{\sigma_B}$=0.065 ns). A resistive wall current monitor (RWM) is located in the beamline just before the proton target. Figure 1 shows a schematic of the BNB and MicroBooNE detector. The RWM current reproduces accurately the proton pulse longitudinal profile. A typical waveform from the BNB RWM, digitized at 2 GHz is shown in Figure 2. The first bunch of this signal is used to monitor the timing of the accelerator trigger signals at MicroBooNE. Figure 3 shows example waveforms of the digitized RWM signal record with MicroBooNE's PMT electronics.

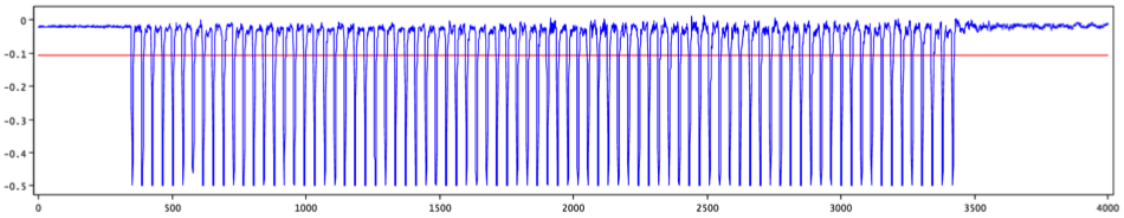

Figure 2: The BNB RWM waveform in blue. Discriminator threshold for oscilliscope in red. Horizontal axis in time-ticks (1 time-tick = 0.5 ns). Vertical axis is the induced charge on the RWM in volts. The BNB proton pulse length is ~1.6 μs, each bunch of protons is spaced at ~18.9 ns, within the pulse [5].

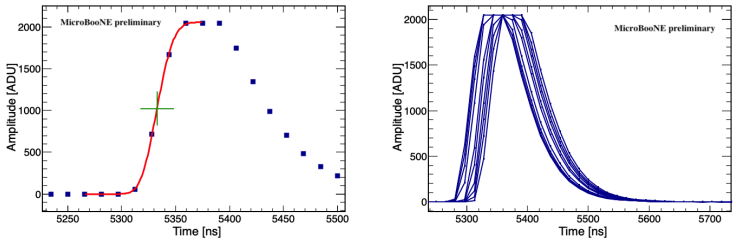

Figure 3: Left: the RWM logic pulse in coincidence with the first proton bunch from the accelerator, recorded by the MicroBooNE DAQ. The red curve shows the waveform rising edge fit, and the green cross marks the rising edge half height point used to assign the timing to the RWM pulse. Right: Multiple RWM logic pulses are reported to show the main trigger jitter. The signal timing is given in the waveform reference frame (t=0 is the first tick of the 1500 ticks of each waveform, each tick is 15.625 ns).

3 PMTs and RWM signals timing

The 32 PMTs (of which 1 channel is unresponsive starting in the summer of 2017), composing the MicroBooNE PDS provide a prompt response to the scintillation light produced in neutrino interactions, Figure 4 shows example traces of candidate neutrino interactions recorded with the MicroBooNE PDS. In coincidence with the BNB trigger, 31, 23.4 μs long waveforms are recorded. PMT pulses are smoothed by an analog unipolar shaper of 60 ns rise time and then digitized at 64MHz (16.625 ns samples). Despite the relative small sampling frequency, the event start time can be determined with a higher timing resolution leveraging the pulse rise time, see Figure 4 right. The upper limit for the pulse timing uncertainty is estimated to be $\sigma_t \simeq 0.2$ ns, as shown in Figure 5 right, negligible compared to the overall resolution of $\mathcal{O}(1)$ ns achieved.

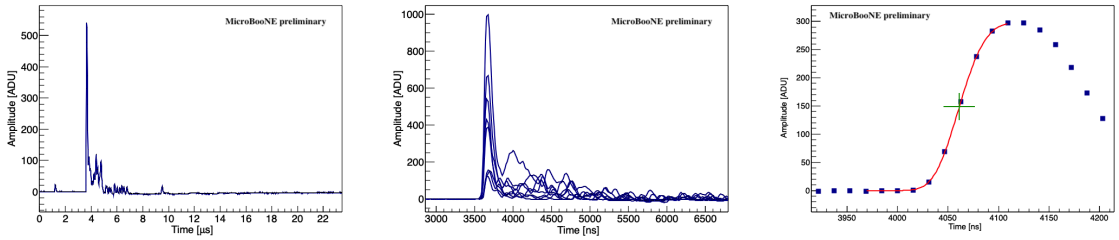

Figure 4: Left: PMT pulse acquired at 64 MHz. Each waveform has 1500 ticks, each tick is 15.625 ns. Center: Multiple PMT pulses for a candidate neutrino interaction event. Right: Single PMT pulse timing extraction. The red curve shows the pulse rising edge fit, and the green cross marks the rising edge half height point used to assign the timing to the PMT pulse. Note: the three pictures shows single/multiple waveforms from three different events.

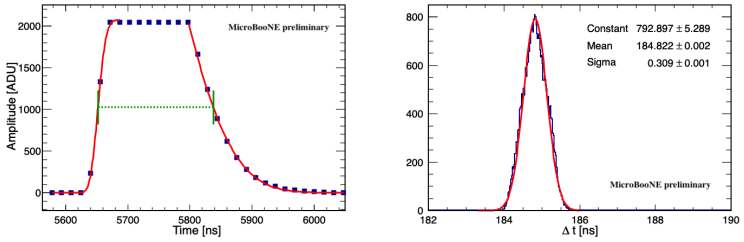

Figure 5: Left: single RWM pulse with rising and falling edge fits, green dotted line shows the pulse half height width. Right: Gaussian fit of the pulse half height width distribution. This distribution is used to estimate the uncertainty of the fitting method ($\sigma/\sqrt{2}$).

4 BNB timing reconstruction from PDS signals

The MicroBooNE timing resolution for neutrino interaction events is evaluated reproducing the BNB ns substructure using the scintillation light prompt signal detected by the PDS. The reference for the beam pulse timing profile is provided by the RWM. Immediately before hitting the target, protons cross the RWM, inducing a current on it, reproducing the proton pulse longitudinal profile, see Figure 2. Between the signal induced by protons at the RWM, and the signal provided by PMTs, there is a complex chain of processes to take into account in order to extract the neutrino interaction timing. The time required for protons to hit the target, the intermediate propagation of mesons and their decay to neutrinos, and the travel time of neutrinos to the detector is assumed to be the same for all events, and is therefore treated as a constant offset for all interactions. This is found to be a good approximation for the neutrinos selected in this analysis. Below we describe the chain of corrections applied once neutrinos enter the TPC.

4.1 ToF corrections

After reaching the TPC upstream wall, neutrinos travel inside the argon medium and eventually they can interact with with an argon nucleus, producing daughter particles which travel a certain path losing energy. Figure 6 shows the 3D view of reconstructed tracks (black points) in a ν_μCC event. Leveraging the information about the neutrino interaction vertex position [6] and the reconstructed daughter particles tracks geometry [7], the processes inside the TPC are reconstructed and the delay due to the particle or light propagation is removed.

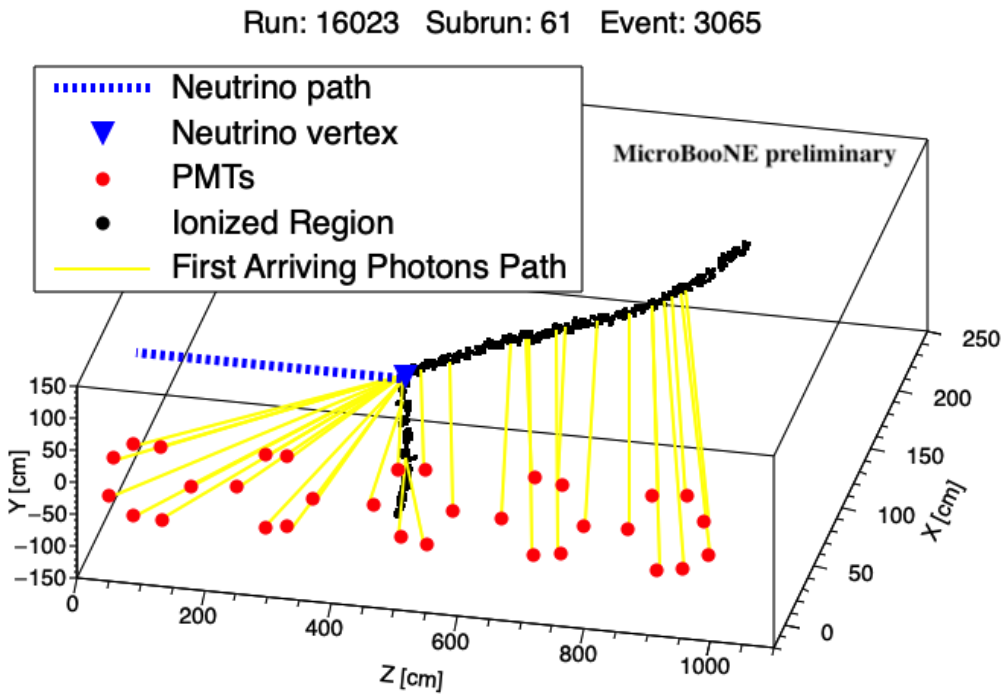

Figure 6: 3D view of a ν_μCC event reconstructed track using Pandora [7], black points. Red points show the PMTs position. In blue the reconstructed neutrino vertex [6] and path. Yellow lines are the path of the first photons arriving on each PMTs. Based on the track geometry, and the PMTs position, for each PMT there is a different space-point as source for the first arriving photons.

Three processes are identified to reconstruct the chain from the neutrino crossing the upstream wall of the detector to the photons reaching the PMTs:

- the neutrino propagation inside the TPC

- the daughter particle propagation from the neutrino interaction vertex to the position where photons are produced
- the scintillation light propagation from the position where photons are produced to the PMT where photons are detected

Since the beam is on-axis with the detector (along z direction), the distance travelled from the TPC upstream wall (z=0) to the reconstructed neutrino interaction vertex (x,y,z), is equal to z. Neutrinos propagate at the speed of light in vacuum giving a neutrino ToF (ν_{ToF}) of z/c. The light source (coincident with the daughter particle track) can extend for meters inside the TPC. Both the ToF of the daughter particle and the ToF of the scintillation photons changes for each space-point along the track. Using the group velocity (v_g), $1/v_g$=7.46±0.08 ns/m [8], for the scintillation light propagation in liquid argon, and c for the daughter particle propagation, an overall propagation time (pt_j) for each space-point is defined as the sum of the daughter particle ToF plus the scintillation photons' ToF. The PMT signal timing obtained from the pulse-fitting method is sensitive to the first arriving photons. The overall propagation time associated to the first photon arriving (pt^*) is motivated by the interest in recording the first photons to arrive. Given the interest in measuring the first photons to arrive, Rayeligh scattering is neglected in these corrections. Note that in a given event each PMT pulse timing has a different pt^* value for the ToF reconstruction, based on the PMT location.

5 Neutrino event timing

For each given event, the trigger jitter (t_{RWM}) and the reconstructed propagation (ν_{ToF}+pt^*) are removed from the timing measured by each PMT. Once the combined daughter particle and scintillation light propagation is removed, all PMTs should give equivalent timing measurements for a given neutrino interaction event. The median time of all measured times across PMTs which collect more than two PEs is chosen as the interaction time. Figure 7 shows the neutrino interaction timing before and after the beam reconstruction.

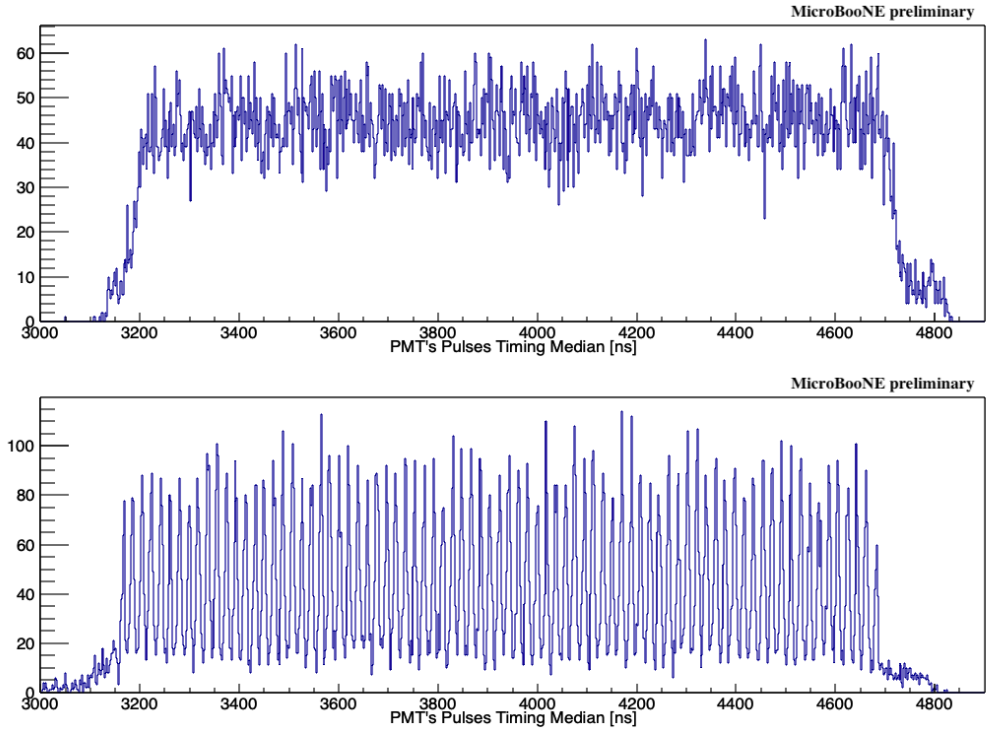

Figure 7: Top: neutrino interaction timing distribution before the reconstruction. Bottom: neutrino interaction timing distribution after the reconstruction. The 81 bunches composing the ∼1.6 μs beam pulse sub-structure are well visible after the reconstruction.

6 Measurement of bunch timing structure

The reconstructed neutrino interaction timing distribution of Figure 7 (bottom) reproduces accurately the RWM waveform structure shown in Figure 2. A Gaussian fit of the 81 bunches is performed and the peaks mean is used to measure the bunch separation. The linear fit in Figure 8 left gives 18.936±0.001 ns for the bunch separation, matching the expectation from the accelerator frequency parameter (see Section 2). The 81 bunches are merged in a single peak, accounting for their offset from the fit, as shown in Figure 8 right. To evaluate the timing resolution, the "superimposed" peak is fitted with a function composed of a central Gaussian, of which the fit parameter σ characterizes the timing resolution, and two further identical Gaussian functions with the mean shifted by the bunch separation, to account for tails from the previous and next bunch peaks in the beam pulse structure. Finally an overall constant term accounts for a flat background from cosmic events.

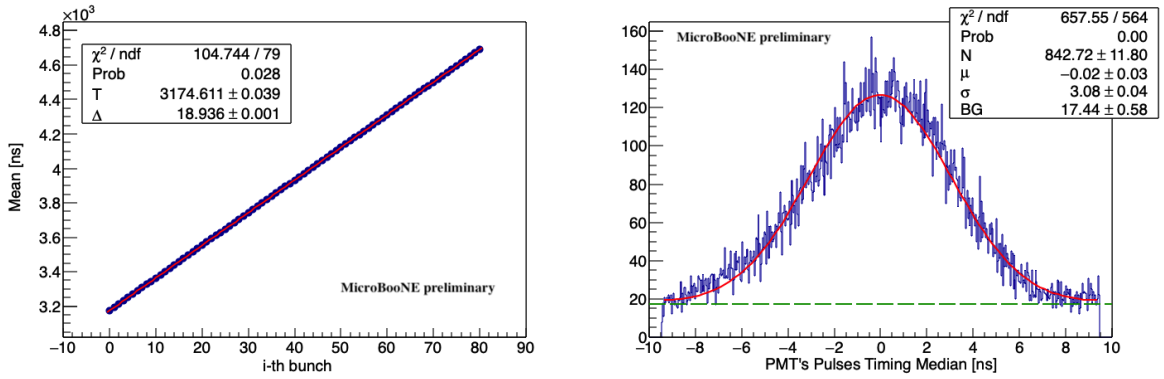

Figure 8: Left: the mean of a Gaussian fit made for each of the 81 bunches, is used to find the bunch separation through a linear fit. Right: the linear fit's constant term and slope are used to merge the 81 bunches in a unique peak.

7 Empirical corrections

Offset corrections and an empirical calibrations are applied to improve the uniformity of the detector response. For these corrections, timing information from each PMT is considered, rather than the median value across PMTs. The pulse timing obtained from each PMT passing several outlier cuts is shifted to have all the bunches merged in a single peak. Then the timing distribution is subdivided into:

- PMT number
- pt*: propagation time of the daughter particle plus scintillation light from the neutrino vertex to a given PMT
- N_{Ph}: number of detected photons by a given PMT.

Distributions of PMT, pt* and N_{Ph} are reported in Appendix 5, Figure 22.

7.1 PMT by PMT offset

The time distribution given by each PMT is analyzed to check for a possible PMT by PMT offset due to electronics, signal transmission or other intrinsic delays. Each single PMT timing distribution is fitted using the same method of Sec. 6 and the mean of the central peak is used to estimate the offset. Figure 9 left shows the measured offset. Once the PMT offset is removed the median is again used to estimate the event timing. The event timing distributions after the offset removal is shown in Figure 9 right (each single PMT timing distributions is reported in Appendix 1: Figue 14 and Figue 15).

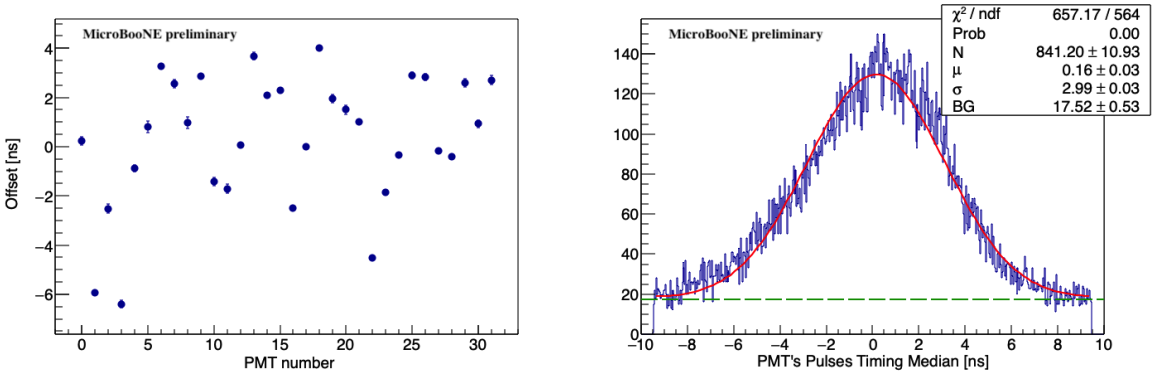

Figure 9: Left: mean from the fit of each single PMT timing distribution. Right: event timing distribution (using the PMTs median) after the offset is removed by each PMT.

7.2 Propagation correction

A study of the event timing uniformity across the detector volume is made. The interaction timing distribution is broken up based on the pt* and N_{Ph} values (timing distributions broken up for pt* and N_{Ph} and the correlation pt* vs. N_{Ph}, are reported in Appendix 5, Figure 22). For each subgroup of events in a given interval of pt* and N_{Ph} the timing distribution is fitted using the same method of Section 6. The mean values are then used to find the empirical factors PT and DP given by the slope of the fits shown in Figures 10 left and Figures 10 center. A correction factor:

$$CF(pt^*, N_{Ph}) = PT \cdot pt^* + DP \cdot N_{Ph} \quad (1)$$

depending on both variables, is removed by each single PMT timing measurement. The median is again used to estimate the event timing. The new event timing distributions after correcting for the offset and the empirical calibration, CF(pt*,N_{Ph}), is reported in Figure 10 right.

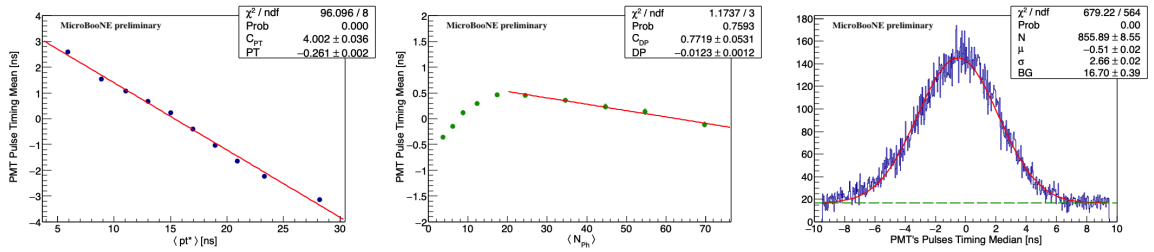

Figure 10: Left: PMT timing as function pt*. Center: PMT timing as function of N_{Ph}. Right: event timing distribution after correcting for the PMT by PMT offset and the CF(pt*,N_{Ph}).

7.2.1 Iterating the calibration process

Once the correction factor is applied to each PMT timing, the new timing distribution is again analyzed with the same procedure to obtain an updated correction factor. This process is applied recursively. Cumulative values for PT and DP and the σ of the event timing distribution versus number of iterations (n) are shown in Figure 11 left, center and right. The values DT=0.523 [ns]/[ns] and PT=0.0648 [ns] used for the final corrections are obtained after nine iterations. The final event timing distribution is reported in Figure 12 left.

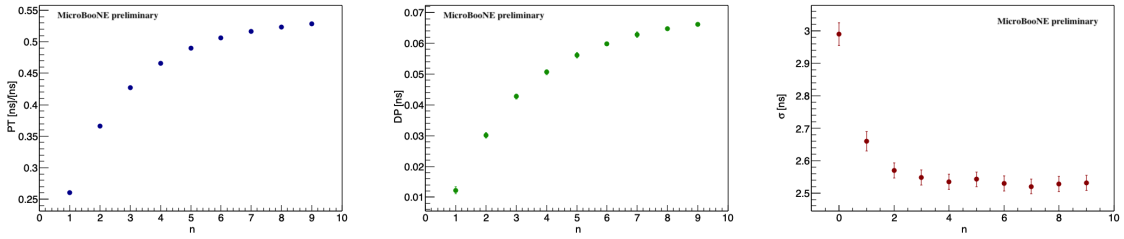

Figure 11: Left: PT cumulative values versus number of iterations (n). Center: DP cumulative values versus number of iterations (n). Right: event timing spread versus number of iterations (n).

8 Detector timing resolution

Once all the reconstruction steps are implemented and corrections applied, the neutrino candidate timing distribution, reported in Figure 12 left, is used to extract the PDS timing resolution for neutrino interactions. To obtain the final calibrated timing resolution, the beam bunches width, $\langle\sigma_B\rangle \simeq$1.308 ns, is subtracted from the measured timing distribution width, σ=2.53±0.02 ns, obtaining the final value for the overall detector timing resolution (R_{Tot}) for ν_μCC candidate events:

$$R_{Tot} = \sqrt{\sigma^2 - \sigma_B^2} = \sqrt{2.53^2 - 1.31^2} = 2.16 \pm 0.02\, ns \tag{2}$$

8.1 Detector intrinsic timing resolution

A characterization of the timing resolution versus the total number of detected photons is made. The parameter σ versus the total number of detected photons, shown in Figure 12 right, is fitted using the function:

$$\sigma\left(\langle N_{Ph}\rangle\right) = \sqrt{k_0^2 + \left(\frac{k_1}{\sqrt{\langle N_{Ph}\rangle}}\right)^2} \tag{3}$$

The k_1 parameter is associated to the statistical uncertainty ($\propto \sqrt{N_{Ph}}$). The constant term k_0, independent of the number of photons detected, is associated with the intrinsic resolution. As for R_{Tot}, the beam bunch width is subtracted from k_0 obtaining the final value for the intrinsic detector timing resolution (R_{Int}) for ν_μCC candidate events:

$$R_{Int} = \sqrt{k_0^2 - \sigma_B^2} = \sqrt{2.17^2 - 1.31^2} = 1.73 \pm 0.04\, ns \tag{4}$$

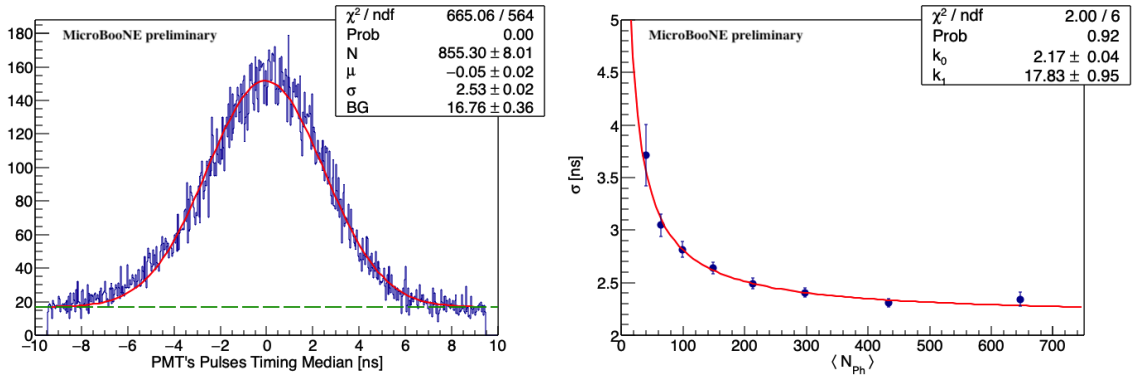

Figure 12: Left: event timing distribution after reconstruction steps removed and corrections applied. The green dotted line shows the constant term, associated to the cosmic background uniform contribution. Right: resolution as function of the total number of photons detected.

9 Background rejection

The achieved timing resolution makes it possible to exploit the timing of the neutrino interaction to remove a fraction of cosmic background events from the BNB's neutrino candidates. This is possible since cosmic events arrive uniformly in time while BNB's neutrinos follow the proton pulse structure. Using a cut demonstrated in Figure 13 left, a selection window around the peak mean of the BNB's superimposed bunches can be used to reduce the fraction of cosmic background events. Figure 13 center shows the fraction of background rejected and the fraction of beam neutrinos preserved as function of a selection window width. Finally, Figure 13 right shows the direct dependence of the neutrino efficiency versus the background rejection. Neutrino efficiency and background rejection values for the three cuts ($\pm\sigma$,$\pm 2\sigma$,$\pm 3\sigma$) are summarized in Table: 1.

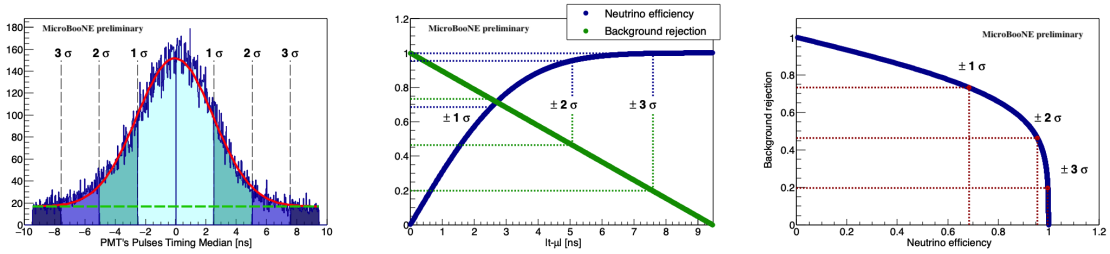

Figure 13: Left: event timing distribution with three selection windows ($\pm\sigma$,$\pm 2\sigma$,$\pm 3\sigma$) around the peak mean. Center: fraction of background rejected (green) and fraction of beam neutrino preserved (blue) as function of a selection window width. Right: the neutrino efficiency versus background rejection.

Cut	$\frac{Cut}{width}$ [ns]	BG_{Tot} (%)	ν_{eff} (%)	BG_{rej} (%)
No cut	18.936	27.1	100	0
$\pm 3\sigma$	15.18	21.7	99.7	19.8
$\pm 2\sigma$	10.12	15.2	95.5	46.6
$\pm\sigma$	5.06	10.6	68.3	73.3

Table 1: Estimated total background (BG_{Tot}), neutrino efficiency (ν_{eff}), and background rejected (BG_{rej}) vs. cut width.

References

[1] R. Acciarri et al. Design and Construction of the MicroBooNE Detector. JINST, 12(02):P02017, 2017.

[2] S. Pate et al. A Model for the Global Quantum Efficiency for a TPB-Based Wavelength-Shifting System used with Photomultiplier Tubes in Liquid Argon in MicroBooNE. JINST, 13(02):P02034, 2018.

[3] Wouter Van De Pontseele. Search for electron neutrino anomalies with the microboone detector. FERMILAB-THESIS-2020-11, 10.2172/1640226, Oxford U., 2020.

[4] A. A. Aguilar-Arevalo and others. Neutrino flux prediction at miniboone. Phys. Rev. D, 79:072002, Apr 2009.

[5] A. A. Aguilar-Arevalo et al. Dark matter search in nucleon, pion, and electron channels from a proton beam dump with miniboone. Phys. Rev. D, 98:112004, Dec 2018.

[6] MicroBooNE Collaboration. Reconstruction performance studies with microboone data in support of summer 2018 analyses. MICROBOONE-NOTE-1049-PUB, 2018.

[7] R. Acciarri et al. The Pandora multi-algorithm approach to automated pattern recognition of cosmic-ray muon and neutrino events in the MicroBooNE detector. Eur. Phys. J. C, 78(1):82, 2018.

[8] M. Babicz et al. A measurement of the group velocity of scintillation light in liquid argon. JINST, 15(09):P09009, 2020.

10 Appendices

10.1 Appendix 1: PMT by PMT offset

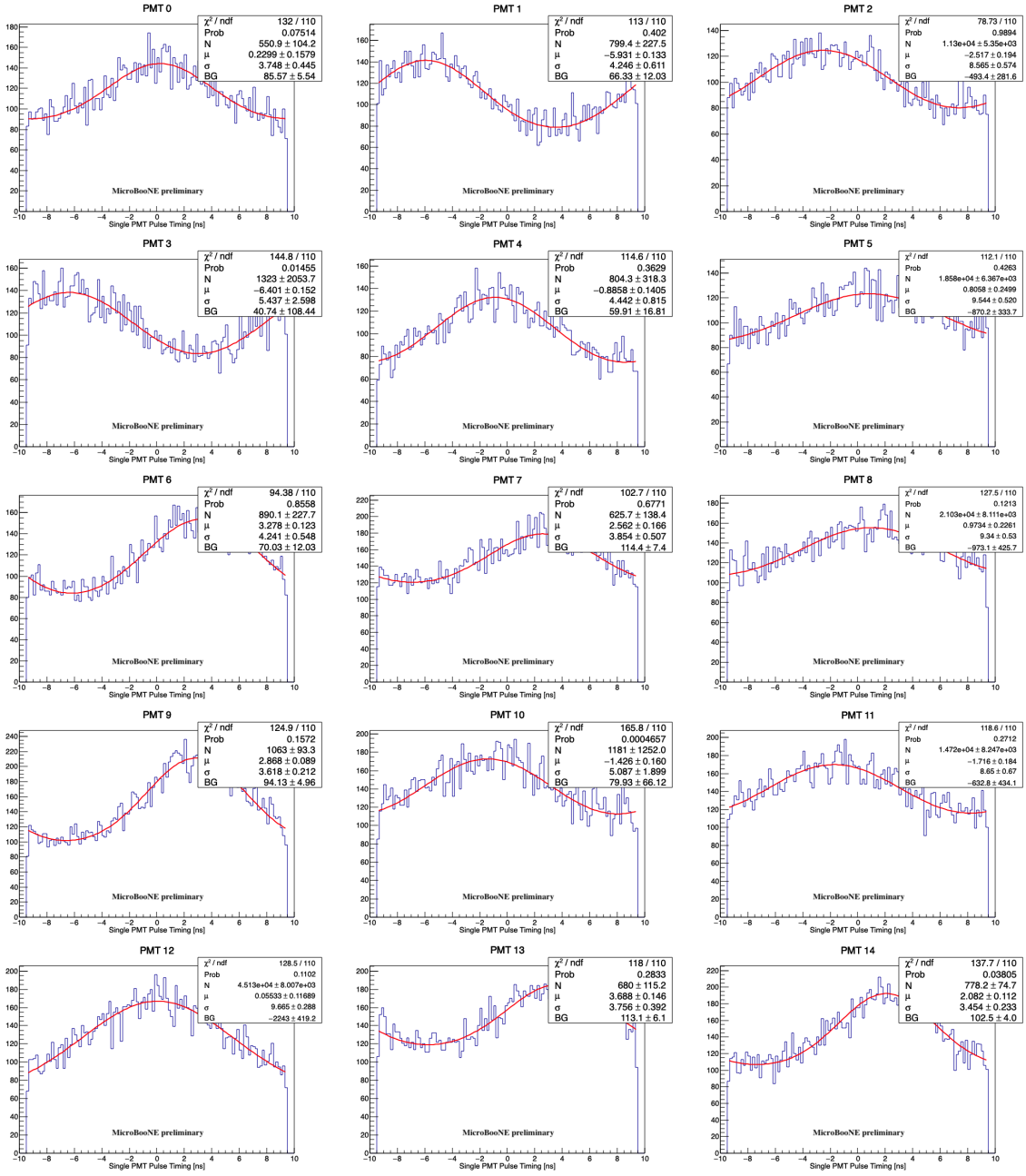

Figure 14: Single PMT timing distribution (PMTs 0 - 14).

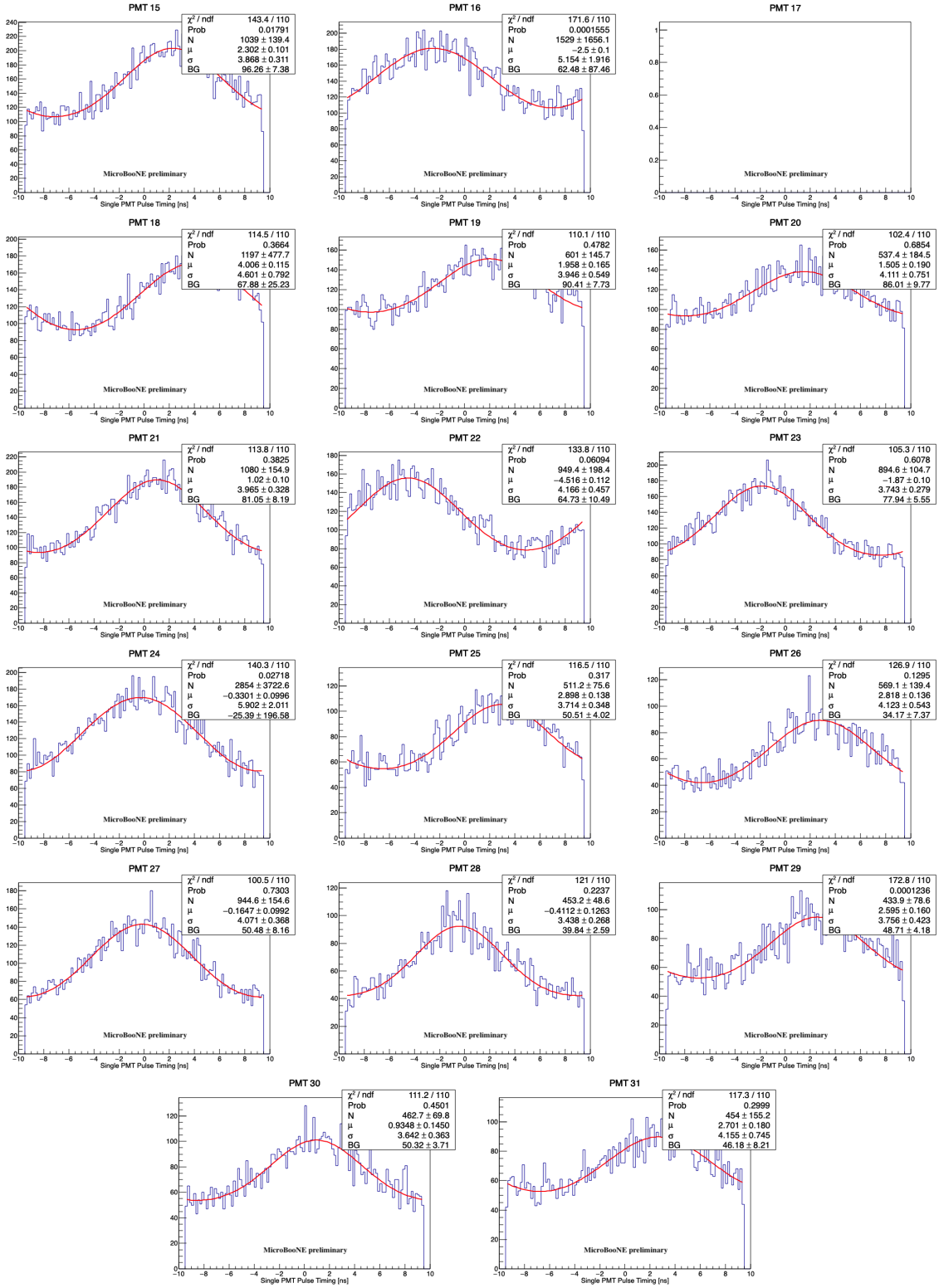

Figure 15: Single PMT timing distribution (PMTs 15 - 31).

10.2 Appendix 2: Step 1 broken up distributions

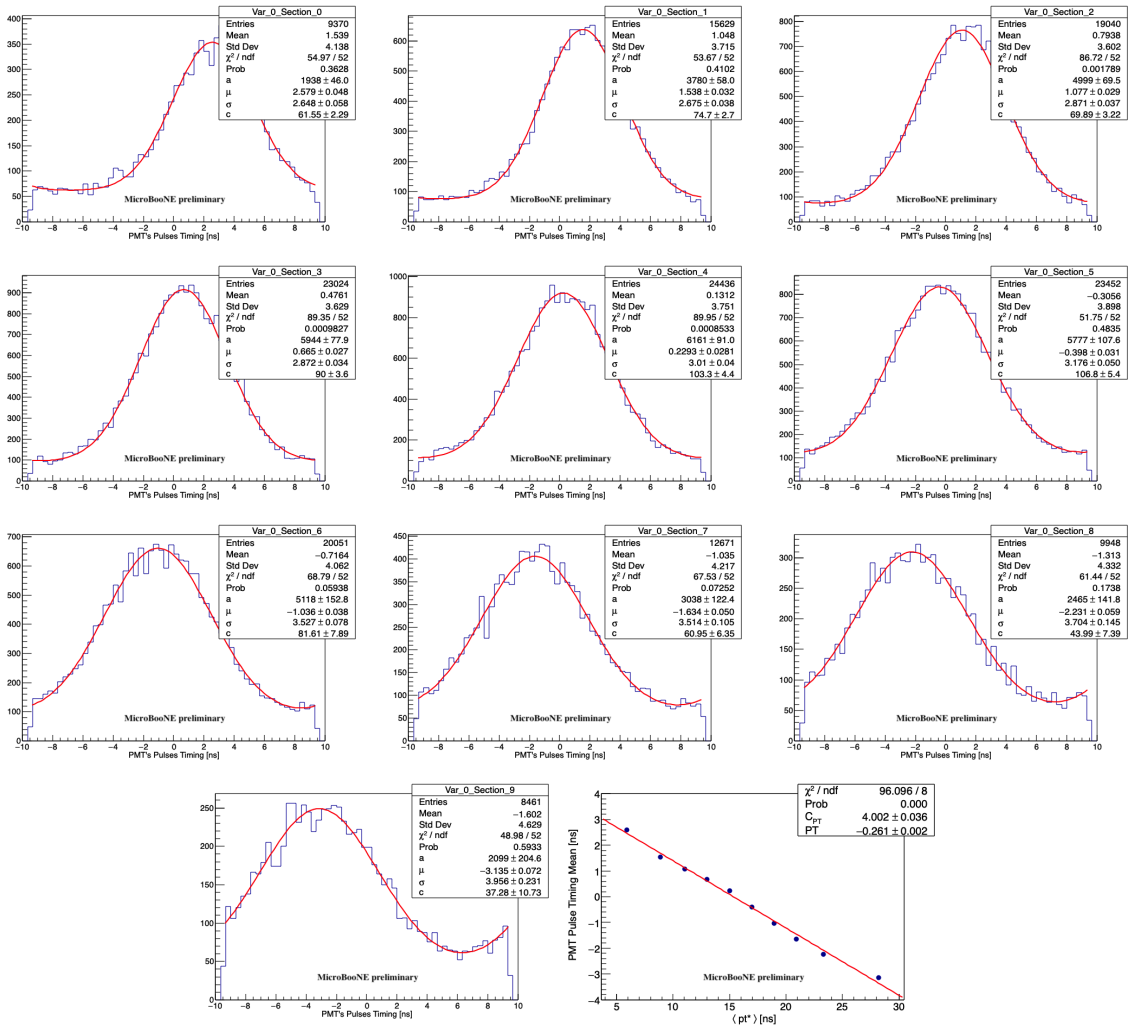

Figure 16: Single PMT timing distributions, broken up for the combined daughter particle and scintillation light propagation. Step 1.

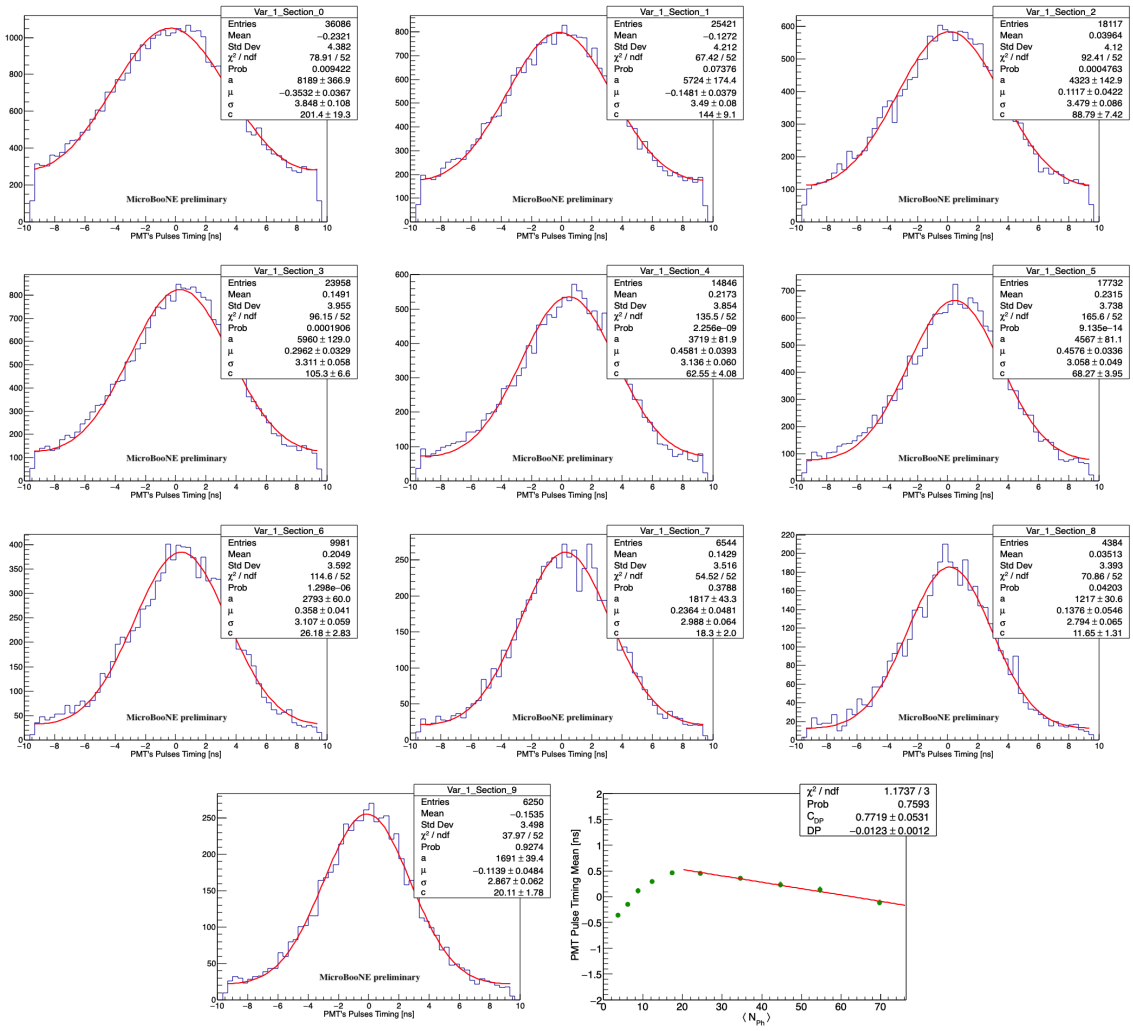

Figure 17: Single PMT timing distributions, broken up for the number of detected photons. Step 1.

10.3 Appendix 3: Calibration Factors Step by Step

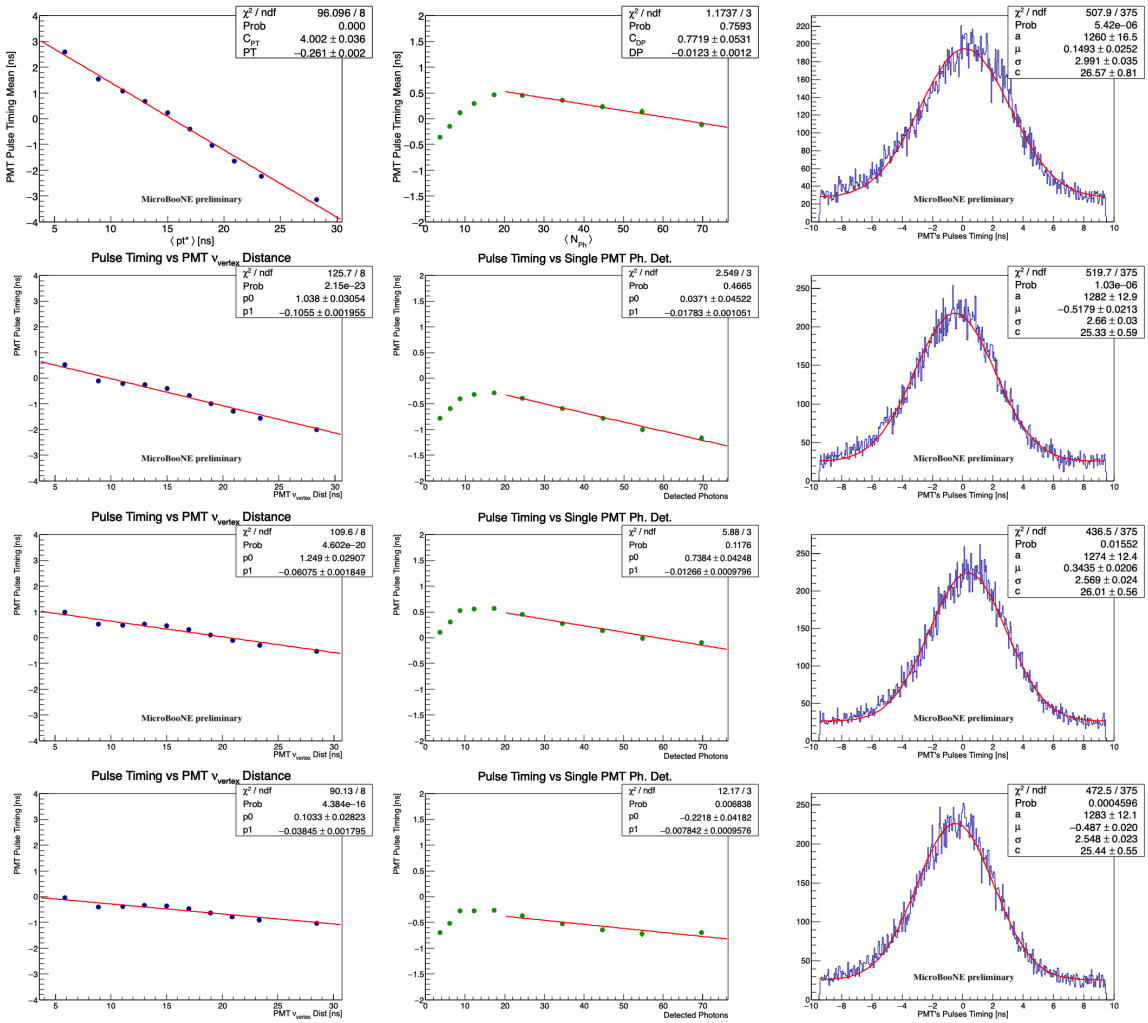

Figure 18: PMT timing as function of daughter particle plus scintillation light propagation, left; and as function of photon detected, center. Timing distribution after correcting for the values found in the fit, right. For Steps from 1 to 4

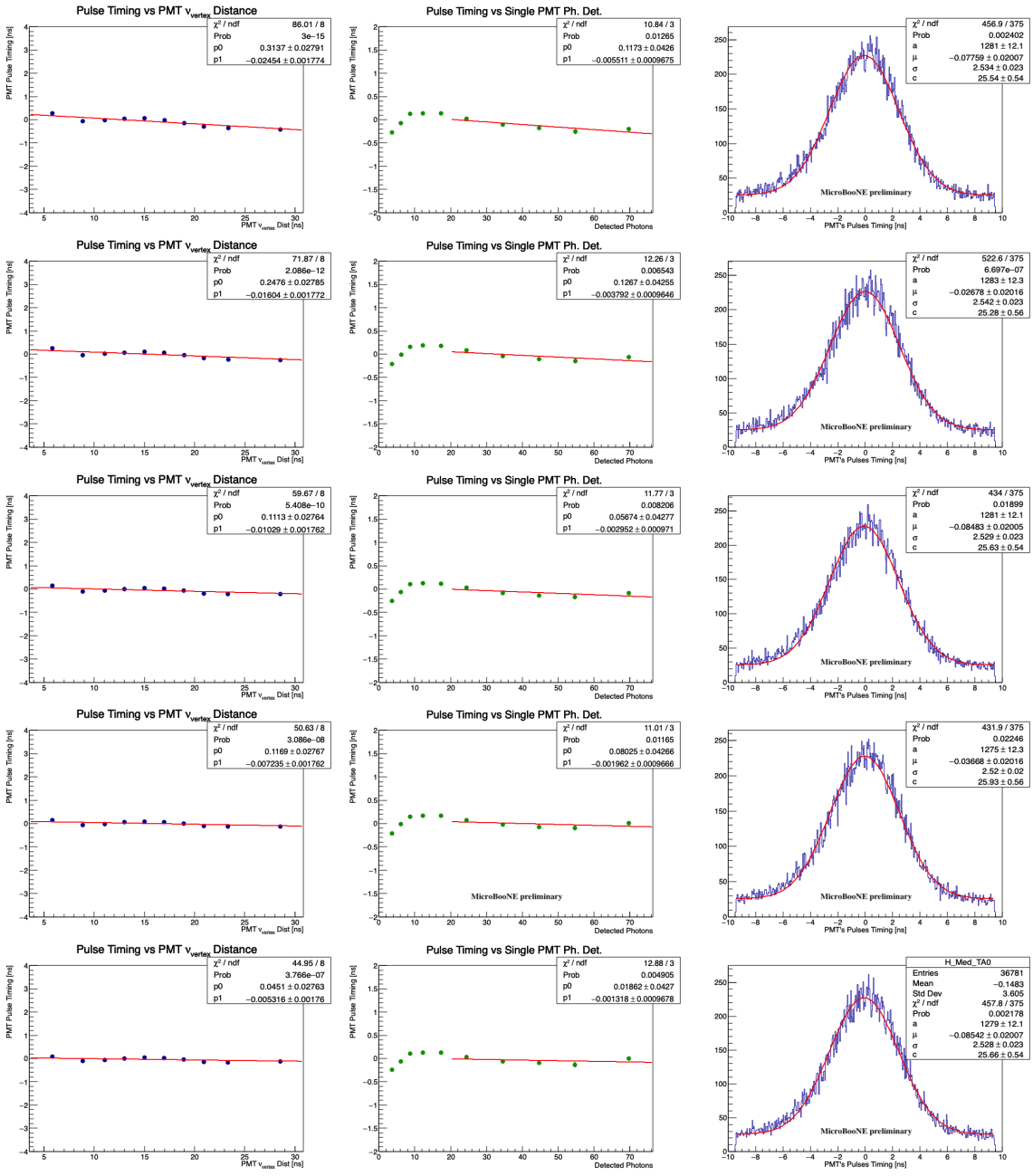

Figure 19: PMT timing as function of daughter particle plus scintillation light propagation, left; and as function of photon detected, center. Timing distribution after correcting for the values found in the fit, right. For Steps from 5 to 9

10.4 Appendix 4: Resolution breaks up

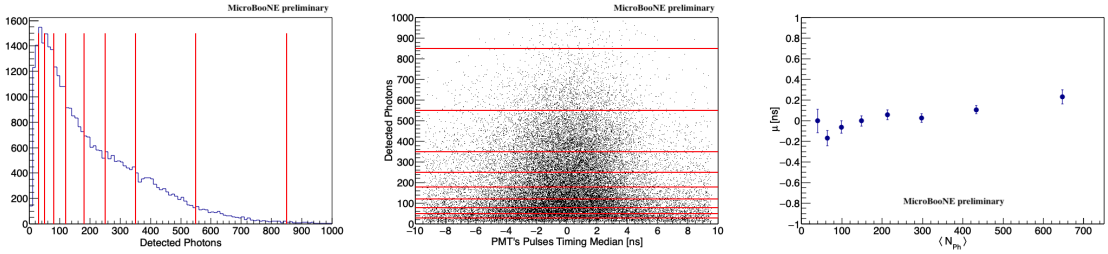

Figure 20: Total number of detected photons, left. Total number of detected photons vs PMTs median timing, center. Mean of the broken up distributions.

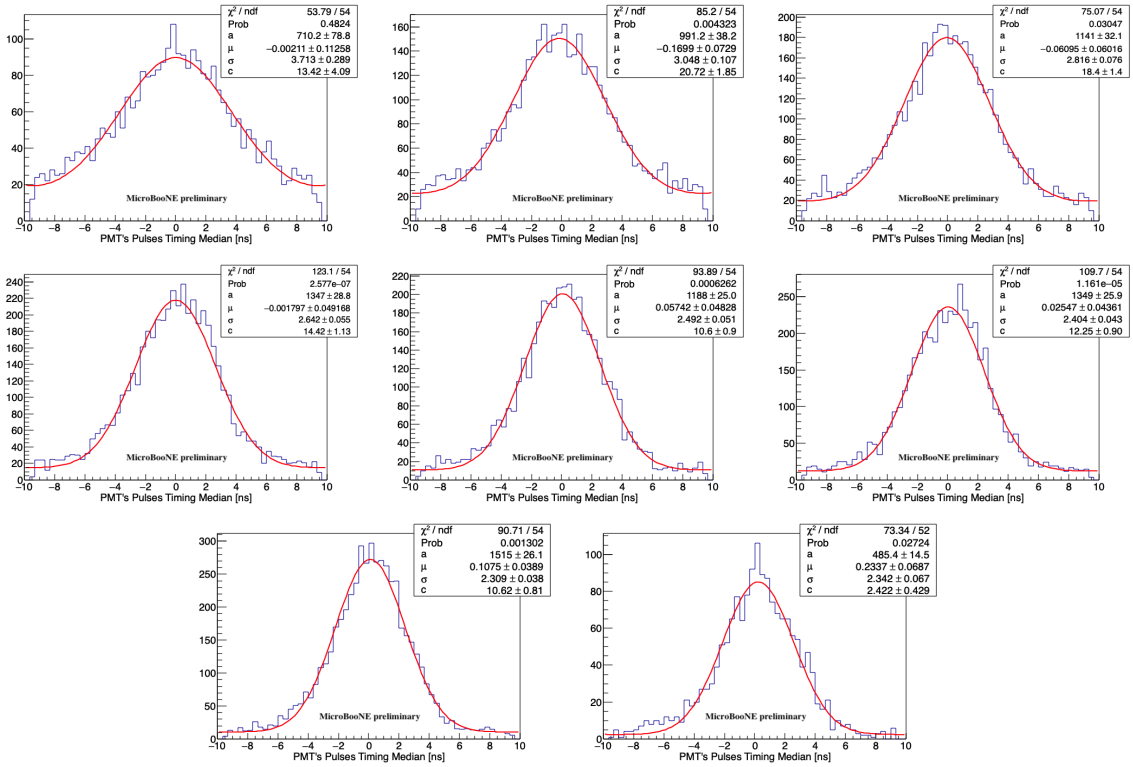

Figure 21: PMTs median timing distribution broken up for the total number of detected photons.

10.5 Appendix 5: Corrections overview

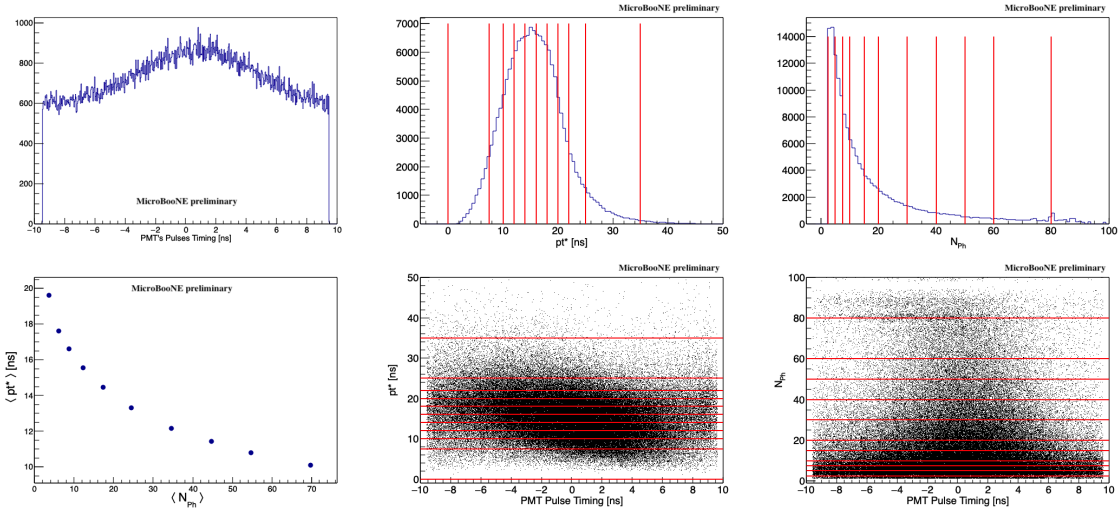

Figure 22: Multiple PMT's timing distribution (top left), propagation time distribution (top center) and number of detected photon distribution (top right). Bottom left: average propagation time versus the average number of photon detected. Bottom center and right: propagation time and number of detected photon distributions broken through the event timing. Red lines delimit groups. The timing distribution of events in each group is fitted with a Gaussian and the mean value versus average number of detected photons or average propagation time from ν vertex to each PMT is used to perform the correction analysis